FULL PAPER

Magnetic Resonance in Medicine 000:000–000 (2012)

MR Imaging of the Amide-Proton Transfer Effect and the pH-Insensitive Nuclear Overhauser Effect at 9.4 T

Tao Jin,[1]* Ping Wang,[1] Xiaopeng Zong,[1] and Seong-Gi Kim[1,2]

The amide proton transfer (APT) effect has emerged as a unique endogenous molecular imaging contrast mechanism with great clinical potentials. However, in vivo quantitative mapping of APT using the conventional asymmetry analysis is difficult due to the confounding nuclear Overhauser effect (NOE) and the asymmetry of the magnetization transfer effect. Here, we showed that the asymmetry of magnetization transfer contrast from immobile macromolecules is highly significant, and the wide spectral separation associated with a high magnetic field of 9.4 T delineates APT and NOE peaks in a Z-spectrum. Therefore, high-resolution apparent APT and NOE maps can be obtained from measurements at three offsets. The apparent APT value was greater in gray matter compared to white matter in normal rat brain and was sensitive to tissue acidosis and correlated well with apparent diffusion coefficient in the rat focal ischemic brain. In contrast, no ischemia-induced contrast was observed in the apparent NOE map. The concentration dependence and the pH insensitivity of NOE were confirmed in phantom experiments. Our results demonstrate that in vivo apparent APT and NOE maps can be easily obtained at high magnetic fields and the pH-insensitive NOE may be a useful indicator of mobile macromolecular contents. Magn Reson Med 000:000–000, 2012. © 2012 Wiley Periodicals, Inc.

Key words: magnetization transfer; chemical exchange saturation transfer; amide proton transfer; nuclear Overhauser effect; MTR asymmetry; ischemia

INTRODUCTION

The exchange of nuclear magnetization between protons of bulk free water and its neighboring molecules in a saturation transfer experiment provides valuable imaging contrasts for MRI. The molecules of interest include metabolites, mobile macromolecules, semisolid macromolecules, and the hydration layer around them. With selective off-resonance irradiation, protons from certain metabolites or macromolecules are saturated and the saturated magnetization can be transferred to the free water via different pathways including intramolecular or intermolecular dipolar cross-relaxation, proton exchange, or molecular exchange, resulting in a reduction of the longitudinal water magnetization. The magnetization transfer (MT) effect can be visualized from the variation of water signal as a function of offset frequency of the irradiation pulse, i.e., the Z-spectrum (1). Conventional MT contrast (MTC) resulting from the semisolid or immobile macromolecules (IMs), denoted as MTC_{IM}, has been developed for many years and applied in MR angiography and pathological studies such as multiple sclerosis (2,3). While MTC_{IM} occurs over a broad range of offset frequencies (on the order of 100 ppm) in the Z-spectrum, the MTC due to mobile macromolecules, denoted as MTC_{MM}, can be detected either by chemical exchange or the nuclear Overhauser effect (NOE) at more specific frequency offsets relatively close (<10 ppm) to the water resonance frequency (see Fig. 1a) and has attracted increasing research interests.

Amide proton transfer (APT) is one variant of the chemical exchange saturation transfer (CEST) contrast (4), referring to the proton exchange between water and backbone amide groups in proteins and peptides (5). The APT contrast has emerged as a sensitive indicator of tissue pH and concentrations of endogenous mobile proteins and peptides and has shown of great potential in stroke and cancer studies (5–11). In an image acquired under irradiation at the amide proton frequency (e.g., 3.6 ppm from water resonance frequency), the signal is decreased not only by the APT effect but also by the direct water saturation (DS) effect and the MTC_{IM}. APT signal is usually assessed from an MTR_{asym} map, i.e., the normalized difference between two images acquired at the amide proton frequency (e.g., 3.6 ppm) and at the reference frequency (e.g., −3.6 ppm), in an attempt to minimize both DS and MTC_{IM} effects:

$$MTR_{asym}(\Omega) = \{S(-\Omega) - S(\Omega)\}/S_0, \quad [1]$$

where Ω is the radiofrequency (RF) offset from the water, and S_0 is the signal intensity without irradiation. Unfortunately, the MTC_{IM} in tissue is asymmetric around the water proton resonance frequency (5,12), leading to negative background signals in the MTR_{asym} maps. Indeed, it has been shown that the magnitude of MTR_{asym} is much larger than the APT effect at an ultrahigh field of 9.4 T (13). As MTR_{asym} signal is confounded, the characterization of APT effect in previous APT studies, such as the determination of the exchange rate and optimization of the irradiation pulse power, is often derived from a disease model, e.g., the magnitude of APT is determined from the difference of MTR_{asym} at the lesion site versus the contralateral normal region, or from normal versus postmortem animals, assuming other signal

[1]Neuroimaging Laboratory, Department of Radiology, University of Pittsburgh, Pittsburgh, Pennsylvania, USA.

[2]Department of Neurobiology, University of Pittsburgh, Pittsburgh, Pennsylvania, USA.

Grant sponsor: NIH; Grant numbers: EB008717, EB003324, EB003375, and NS44589.

*Correspondence to: Tao Jin, Ph.D., Department of Radiology, University of Pittsburgh, 3025 E Carson Street, Room 156, Pittsburgh, Pennsylvania 15203. E-mail: taj6@pitt.edu

Received 17 January 2012; revised 17 March 2012; accepted 6 April 2012.

DOI 10.1002/mrm.24315

Published online in Wiley Online Library (wileyonlinelibrary.com).

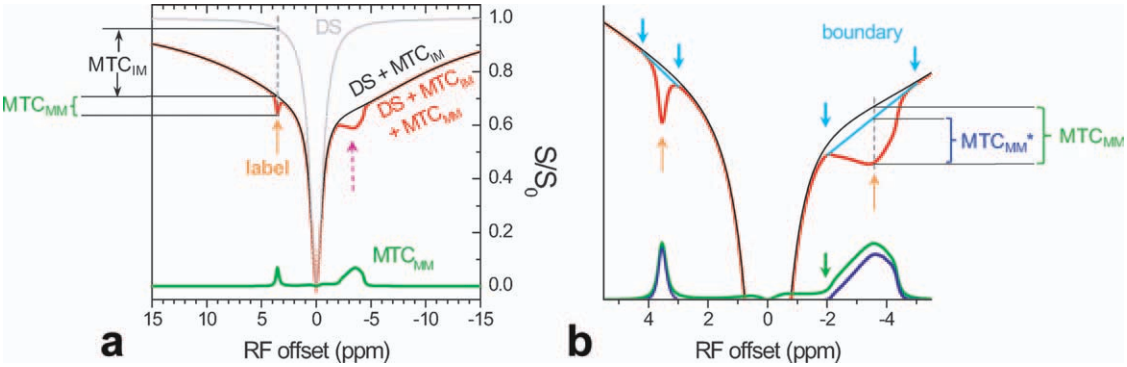

FIG. 1. **a**: Schematic comparison of Z-spectrum with direct water saturation (DS) effect only (gray), both DS and the magnetization transfer contrast from immobile macromolecules (MTC_{IM}) (black), and DS, MTC_{IM}, and the magnetization transfer contrast from mobile macromolecules (MTC_{MM}) effects together (red). At the label frequency (brown arrow), the MT signal can approximately be decomposed into DS, MTC_{IM}, and MTC_{MM} contributions. The reference frequency on the opposite side of the water resonance (dashed arrow) used for MTR_{asym} has different MTC_{IM} and MTC_{MM} contributions. Theoretically, MTC_{MM} signal (green) can be determined from the difference of black and red curves but the practical implementation is difficult. If MTC_{MM} is narrow and its boundaries are well defined (cyan arrows in **b**), then DS+ MTC_{IM} spectrum (black) within the boundaries can be approximated as linear (cyan line segments in b). Its difference with the red spectrum gives an apparent MTC_{MM} (MTC_{MM}*, blue), the error of which is dependent on whether the MTC_{MM} feature is broad (positive vs. negative offsets, b), the separation from the water resonance, and whether the boundary image has residual MTC_{MM} effects (e.g., green arrow).

contributions to the MTR_{asym} remain the same. For example, Zhou et al. estimated an APT magnitude of 2.9% for live animals and 1.04% postmortem based on the observed APT change of −1.86% between the two states (5), and Sun et al. reported a maximum APT contrast of ∼ 2.9% between focal ischemic and normal hemisphere regions at 4.7 T (14). While these successful efforts are based on regional analysis, quantitative imaging of APT is still challenging, especially for pathological conditions with strong regional APT heterogeneities.

NOE has been explored in NMR spectroscopy as an important tool for characterizing chemical structure and determining the biomacromolecular conformation (15–17). Recently, in several in vivo MRI studies with magnetic fields of 7 T or above, significant MT features have been observed in the upfield frequencies, i.e., negative frequency offset from water (13,18–20), likely reflecting a MT process between water and protons from the side groups of large mobile macromolecules, such as the aliphatic components of peptides, proteins, and lipids (21,22). The observation of NOE in MRI at high fields is facilitated because the higher magnetic field slightly increases the magnitude of NOE (as well as APT) due to its proportionality to water T_1, and also increases the spectral separation, leading to the reduction of the DS effect and a better defined NOE feature (as well as APT peak) (13,23). The aliphatic proton frequency of mobile macromolecules observed by NMR spectroscopy spans a range of a few ppm upfield, e.g., about −0.7 to −5 ppm in myosin from rabbit skeletal muscle (24) and cat brain (25), and −0.3 to −3.9 ppm in perfused cancer cells (26). If it is significant, NOE at upfield frequencies (e.g., −3.6 ppm) is clearly a nuisance for the quantification of APT using the asymmetry analysis approach.

Although not a chemical exchange, the spin exchange of NOE can be described by the same mathematical model, thus its signal characteristics would be similar to APT in a saturation transfer experiment (27). The NOE signal should be proportional to the mobile macromolecular concentration as well as the MT rate, which could potentially be exploited as a novel imaging index complementary to APT. However, little has been reported regarding some important properties of the in vivo NOE signal, especially whether it is sensitive to pH. One possible mechanism for in vivo NOE is an exchange-relayed pathway where the saturated magnetization of aliphatic protons is first transferred to neighboring labile amide, hydroxyl, or amine protons, and then transferred to free water via chemical exchange, and it has been suggested that such an exchange-relayed mechanism of NOE may be dominant (28). A dominant exchange-relay pathway would imply a possibility that NOE signal can be sensitive to pH (29). Thus, it is critical to evaluate whether the NOE signal would be affected by a change in tissue pH in the physiological range.

In this work, we reported a simple three offset measurement approach for high-resolution (HR) in vivo mapping of APT and NOE at 9.4 T. Three offset frequencies were selected; one at the center frequency of the APT or NOE peak, while the other two are at the upper and lower bounds of the peak. The signal difference between the peak of interest and the mean of the two bounds approximates true APT or NOE and are dubbed as apparent APT (APT*) or apparent NOE (NOE*). The APT* and NOE* maps measured by the three offset approach were compared with MTR_{asym} and apparent diffusion coefficient (ADC) maps in normal and ischemic rat brains. The dependence of the APT* and NOE* on the irradiation pulse power was also investigated. Finally, the concentration dependence and the pH independence of the NOE signal were validated in protein phantoms.

METHODS

Three Offset Measurement of MTC_{MM}

The signal contributions from DS, MTC_{IM}, and MTC_{MM} to a Z-spectrum are schematically plotted in Fig. 1a. The DS (gray line) mainly affects the RF offsets close to the

water resonance. The addition of MTC_{IM} effect (black line) induces significant signal drop for a wide offset range, which is also asymmetric around the water resonance frequency. At very high magnetic fields, the MTC_{MM}, including the downfield APT and upfield NOE (red peaks), can be delineated by the increased spectral resolution. From Fig. 1, it is apparent that quantitative imaging of either APT or NOE by MTR_{asym} is problematic. Instead, it can be determined from the difference of black and red curves (green, Fig. 1a). In principle, quantification of in vivo APT and NOE can be achieved similarly by fitting a wide Z-spectrum (at least −10 to 10 ppm) to a theoretical model where the DS and the MTC_{IM} effect are taken into account, then subtracting the fitted Z-spectrum from the experimental Z-spectrum. However, the pixel-wise implementation of such a modeling approach is very difficult because of (i) the small magnitude of MTC_{MM} effect versus the large number of fitting parameters involved and (ii) the requirement of large sampling offset frequency points and resultant low signal to noise ratio.

For a well-delineated peak observed at a high magnetic field, we propose that imaging of APT and NOE can be acquired with simple three offset measurements (Fig. 1b). Specifically, the Z-spectrum within two boundary frequencies with minimal MTC_{MM} (cyan arrows, Fig. 1b) can be approximated by linear line segments (cyan lines). This is essentially a simplification of the Z-spectra fitting approach to an extreme where all other effects except the MTC_{MM} of interest are approximated by a linear function. As such, the apparent MTC_{MM} (MTC_{MM}*) calculated from the difference between Z-spectrum and line segments will be an approximation of MTC_{MM} (green vs. blue curves, Fig. 1b). Practically, MTC_{MM}* map can be obtained from a label image at an RF offset of $\Omega = \delta$ with maximum MTC_{MM} and two boundary images with minimum MTC_{MM} and an offset separation of $\pm\Delta$ (Fig. 1b). The MTC_{MM}* at the label frequency can be expressed as:

$$MTC_{MM}^{*}(\Omega = \delta) = \left\{\frac{S(\delta - \Delta) + S(\delta + \Delta)}{2} - S(\delta)\right\}/S_0. \quad [2]$$

Because the frequency offset of the label image with maximum MTC_{MM} is relatively easy to determine, the difference between MTC_{MM} and MTC^{*}_{MM} is mainly dependent on (1) how accurate the two boundary frequencies are chosen, i.e., whether there is residual MTC_{MM} (as shown for one boundary frequency, indicated by the green arrow in Fig. 1b) and (2) how well the Z-spectrum within the two boundary frequencies can be approximated by a linear function. Generally, MTC^{*}_{MM} can be a good approximation if the MTC_{MM} peak is narrow or far away from the water resonance (Fig. 1b). Specifically, for APT* mapping, as will be shown later, can be obtained from a label image acquired at 3.6 ppm and two boundary images acquired at 3.0 and 4.2 ppm:

$$APT^{*} = \left\{\frac{S(3.0\text{ ppm}) + S(4.2\text{ ppm})}{2} - S(3.6\text{ ppm})\right\}/S_0, \quad [3]$$

and the NOE* map can be obtained similarly from three images acquire at −5.0, −2.0, and −3.5 ppm:

$$NOE^{*} = \left\{\frac{S(-5.0\text{ ppm}) + S(-2.0\text{ ppm})}{2} - S(-3.5\text{ ppm})\right\}/S_0. \quad [4]$$

Equations [2–4] assume that the two boundary images have an equal offset shift from the label image, which can be easily extended to a more general case if the two shifts are unequal.

Numerical Simulations

To estimate the error of MTC^{*}_{MM} obtained from three offset measurements (Eq. [2]), numerical simulation of DS, MTC_{IM}, and APT effects were performed with Bloch–McConnell equations. The MT effect between water and protons of IMs (MTC_{IM}) was modeled as a super-Lorentzian function (30,31) and incorporated into the simulations following the work of Li et al (32). The time-dependent differential equations were solved in Matlab® 7.0 in a 1 ms step to saturation pulse duration of 3 s. The simulations were performed in the RF offset range of 0–20 ppm, with three B_1 values of 0.6, 1.0, and 1.5 μT. Parameters used for stimulations were: R_1 values of water, amide, and IM protons = 0.5 s^{-1}, water R_2 = 12, 15, and 18 s^{-1}, amide R_2 = 15 s^{-1}, a fractional pool size of amide proton f_{APT} = 0.001 and 0, a chemical shift of amide from water = 3.6 ppm, the exchange rate of amide with water = 30 s^{-1} (5), a fractional proton pool size of IM = 0.05 for gray matter (GM) and 0.08 for white matter (WM), IM proton T_2 = 10 μs, and an exchange rate between water and IM protons = 50 s^{-1} (12). The APT signal was obtained from the difference of the simulated Z-spectrum with $f_{APT} = 0$ and 0.001. For simplicity, symmetry of MTC_{IM} around the water resonance frequency was assumed, and NOE was not simulated due to contributions of many aliphatic, unknown peaks spanning a relatively wide range.

Overview of MR Experiments

All MRI experiments were performed on a 9.4-T/31 cm magnet with an actively shielded 12-cm gradient insert (Magnex, UK) interfaced to a Varian Unity INOVA console. For in vivo experiments, a volume coil excitation and surface coil reception setup was used (Nova Medical, MA). In phantom experiments, a volume coil was used for both transmit and receive (Rapid Biomedical, OH). Magnetic field homogeneity was optimized by localized shimming on a volume of interest using a three-dimensional gradient-echo automated shimming routine. For a typical shimming volume of ~ 20 mm × 20 mm × 6 mm for phantom and 14 mm × 9 mm × 9 mm for in vivo experiments, the water spectral linewidths were 5–10 Hz and 20–30 Hz, respectively. The B_1 field was mapped for calibration of the transmit power (33).

In MT experiments, a continuous wave RF pulse was applied for irradiation at an off-resonance frequency. After the irradiation, crushing gradients were immediately applied to suppress residual transverse magnetization, then the images were acquired with a single-shot spin-echo echo planar imaging sequence. Control images (S_0) were acquired at an offset of 300 ppm for signal normalization.

Table 1
Detailed Parameters of the In Vivo MT Experiments[a]

Experiment #	1.1	1.2	1.3	1.4	1.5	1.6	1.7
Description	Z	Z_{fine}	APT map	NOE map	B_1-dependence	APT map	NOE map
# of animals	6	6	6	6	7	7	7
Animal ID	#1–6	#1–6	#4–9	#4–9	#7–13	#10–16	#10–16
B_1 (μT)	1.25	1.25	1.25	1.25	Varied[b]	1.25	1.25
T_{sat} (s)	3	3	3	3	4	3	3
# of offsets	69[c]	47[d]	4[e]	4[f]	6[g]	4[h]	4[i]
Number of average	5	12	Varied[e]	Varied[f]	Varied[g]	Varied[h]	Varied[i]
Total time (min)	48	71	60	32	62	30	16

[a]In a total of 16 animals, #1–9 are normal rats and #10–16 are MCAO rats.
[b]B_1 = 0.25, 0.32, 0.4, 0.48, 0.64, 0.8, 1, 1.25, 1.6, 2, and 2.5 μT.
[c]Offsets (ppm) = 0, ±1 × (0.25, 0.5, 0.75, 1, 1.25, 1.5, 1.75, 2, 2.25, 2.5, 2.75, 3, 3.2, 3.4, 3.6, 3.8, 4, 4.25, 4.5, 4.75, 5, 5.5, 6, 7, 8, 9, 10, 11, 12, 13, 14, 16, 18, 20).
[d]Offsets (ppm) = (5, 4.8, 4.6, 4.4, 4.2, 4.0, 3.9, 3.8, 3.7, 3.6, 3.5, 3.4, 3.3, 3.2, 3.1, 3.0, 2.8, 2.6, 2.4, 2.2, 2.0, −1.8, −2.0, −2.2, −2.4, −2.6, −2.8, −3.0, −3.2, −3.4, −3.6, −3.8, −4.0, −4.2, −4.4, −4.6, −4.8, −5.0, −5.2, −5.4, −5.6, −5.8, −6.0, −6.25, −6.5, −6.75, −7.0).
[e]For offsets of 4.2, 3.6, 3.0, and −3.6 ppm, Number of average (NA) = 84, 168, 84, and 144, respectively.
[f]For offsets of −5.0, −3.5, −2.0, and 3.5 ppm, NA = 60, 90, 48, and 60, respectively.
[g]For offsets of 4.2, 3.6, 3.0, −2.0, −3.5, and −5.0 ppm, NA = 5, 10, 5, 5, 10, and 5, respectively.
[h]Same as (*e*) with half NA values.
[i]Same as (*f*) with half NA values.

In Vivo Studies

Animal Preparation

A total of 16 male Sprague–Dawley rats were used with approval from the Institutional Animal Care and Use Committee at the University of Pittsburgh. Rats (weighing between 290 and 480 g) were anesthetized with isoflurane (5% for induction and 2% during surgery) via a vaporizer with a gas mixture of O_2 (30%) and N_2 (70%). The femoral vein was cannulated to deliver pancuronium bromide (0.2 mg/kg/h) and maintenance fluid. The femoral artery was catheterized to monitor the arterial blood pressure and to obtain blood samples for arterial blood gas measurements. For focal ischemia studies, the middle cerebral artery occlusion model (MCAO) was adapted (34). During MRI experiments, the isoflurane level was reduced to 1.3–1.5%, and the dynamic blood pressure and end-tidal CO_2 were monitored. End-tidal CO_2 level was kept within 3.5 ± 0.5%, and the rectal temperature was controlled at 37.2 ± 0.5°C using a water circulating pad.

In Vivo Experiments

Experiments were performed either at HR (Expts. #1.1-1.4), with a field of view (FOV) of 2.56 cm × 2.56 cm, four slices of 1.5-mm thickness, and 0.5-mm gap, or low resolution (LR, Expts. #1.5-1.7), with an FOV of 3.2 cm × 3.2 cm, four slices of 2-mm thickness and no gap. The matrix size was 64 × 64, echo time (TE) was 32 ms for HR and 28 ms for LR, and the postacquisition recovery time, i.e., the time between the acquisition of one MT image and the saturation pulse of the next image, was 3.5 or 4 s. For LR experiments, water saturation shift referencing images were acquired to evaluate the spatial variation of B_0 (35).

Seven types of data were obtained, and their detailed experimental parameters were listed in Table 1. In vivo experiments #1.1–#1.7 are as follows:

(1.1) Whole Z-spectrum was measured in the 20 to −20 ppm offset range, with uneven steps emphasizing the APT and NOE features (n = 6 normal animals).

(1.2) To better characterize APT and NOE effects, Z-spectra were acquired at finer steps and an increased number of averages (NA) to improve the signal to noise ratio (n = 6 normal animals).

(1.3) To obtain MTR_{asym}(3.6 ppm) and APT* maps, MT images were measured at four offsets of 3.0, 3.6, 4.2, and −3.6 ppm (n = 6 normal animals).

(1.4) To obtain MTR_{asym}(5.0 ppm) and NOE* maps, MT images were measured at four offsets of −2.0, −3.5, −5.0, and 5.0 ppm (n = 6 normal animals).

(1.5) To determine the irradiation power dependence of APT* and NOE*, MT images were obtained with eleven B_1 values (n = 7, on three normal and four MCAO rats).

(1.6 and 1.7) To evaluate the imaging contrast of APT*, NOE*, MTR_{asym}(3.6 ppm), and MTR_{asym}(5.0 ppm) in the case of brain ischemia, Expts. #1.3 and #1.4 were performed at LR after 4 h from the onset of MCAO (n = 7 MCAO animals). To identify ischemic regions in MCAO studies, ADC maps were obtained using a multislice spin-echo echo planar imaging sequence, with a low b value of 5 s/mm^2 applied on one axis, and a high b value of 1200 s/mm^2 applied on six different directions.

Phantom Studies

Two types of phantoms were used to characterize NOE signals. Prepared solutions were transferred to cylinders (I.D. = 8.9 mm), which were bundled together for

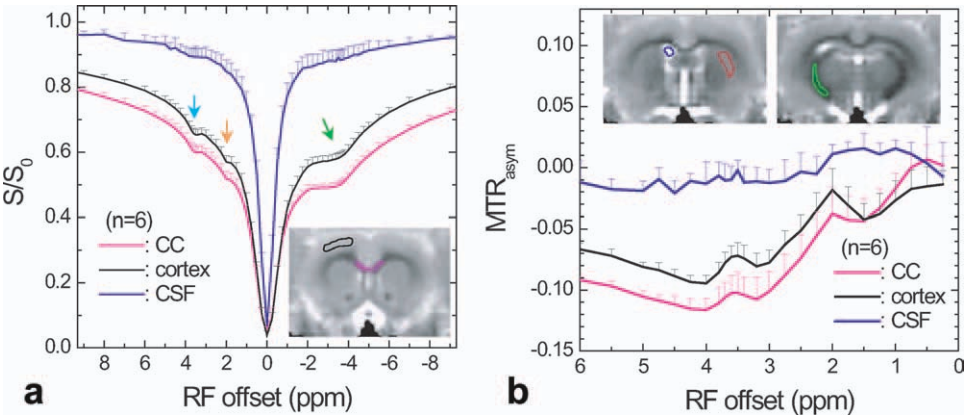

FIG. 2. **a**: The averaged Z-spectrum obtained at cortex, corpus callosum (CC), and cerebrospinal fluid (CSF) ROIs ($n = 6$). **b**: MTR_{asym} shows CEST peaks at 3.6 and 2 ppm on top of the distorted negative background due to the MTC_{IM} asymmetry and NOE effects, which is more prominent in the CC ROI. Insets: three slices of S/S_0 map measured at 5.0 ppm from one representative animal, where the contours of cortex (black), CC (pink), caudate-putamen (red), internal capsule (green), and CSF (blue) ROI were depicted.

imaging. Images were obtained at room temperature with an FOV of 4 cm × 4 cm, slice thickness of 5 mm, matrix size = 64 × 64, TE = 29 ms, and postacquisition recovery time = 10 s. B_0 maps were measured by a multi-TE gradient-echo echo planar imaging sequence. Z-spectra were measured from 8 to −8 ppm range using a 6-s saturation pulse at different B_1 values. Two phantom experiments #2.1–#2.2 are as follows:

(2.1) To study the pH dependence of NOE in proteins, 15% by weight bovine serum albumin (BSA, A7906 from Sigma Aldrich, St. Louis, MO) was dissolved in phosphate buffer saline and titrated to four different pH values of 7.0, 6.4, 5.8, and 5.0. Z-spectra were acquired with B_1 of 0.5 and 1.0 μT.

(2.2) To confirm the dependence of NOE signal on mobile macromolecule concentration, 5, 10, 15, and 20% by weight BSA was dissolved in phosphate buffer saline and titrated to pH = 7.0. Z-spectra were acquired with B_1 of 0.17, 0.35, 0.5, 0.7, 1.0, and 2.0 μT. In addition, MT images were measured by a 0.65 μT and 6 s pulse at three offsets of −2, −3.5, and −5 ppm.

Data Analysis

MTR_{asym}(3.6 ppm) and MTR_{asym}(5.0 ppm) maps were obtained using Eq. [1], and APT* and NOE* maps were calculated with Eqs. [3] and [4], respectively. Quantitative analyses were performed from regions of interest (ROI). To minimize the contamination from B_0 inhomogeneity, the ROIs were selected so that the shift of B_0 from the water resonance frequency was <16 Hz for in vivo data and <3 Hz for phantom data.

In normal animals (Expts. #1.1–#1.5), five ROIs were selected from the S/S_0 map at 5 ppm for the HR data (see Insets, Fig. 2) at the cortex, corpus callosum (CC), caudate-putamen (CPu), internal capsule (IC), and cerebrospinal fluid (CSF) area, whereas two ROIs were selected on the GM and WM areas for the LR data. In the analysis of Expt. #1.5, where four MCAO animals were used, GM and WM ROIs were selected on the contralateral (normal) side. Z-spectrum and MTR_{asym} were obtained from ROIs, and APT and NOE signals were extracted.

In MCAO studies (Expts. #1.6 and #1.7), two ROI in the ipsilateral (ischemic) and contralateral (normal) sides of the CPu area, respectively, and a WM ROI on the contralateral side were selected for quantitative comparison between APT* and MTR_{asym} maps. To compare the regional APT* and MTR_{asym} and their ischemic contrast, a paired Student's *t*-test was used. In addition, one large lesion ROI was selected from the ADC map of each animal from which APT*, NOE*, and ADC values were obtained for pixel-by-pixel correlation analysis. All statistical data in the text and figures are shown as mean ± standard deviation.

RESULTS

In Vivo Regional Z-Spectrum of Rat Brain (Expts. #1.1 and #1.2)

Figure 2a shows the averaged Z-spectra from CSF, cortex, and CC ROIs ($n = 6$, Expt. #1.1) measured with a 1.25 μT and 3 s saturation pulse. Although an offset range of 20 to −20 ppm was acquired, only part of the data was displayed for better visualization of the main features of interest. Both cortex and CC Z-spectra had a small signal dip at ~ 3.6 ppm due to APT effect (cyan arrow) and a broader dip due to NOE at negative frequency offsets (green arrow). The Z-spectrum of the CSF mostly shows the DS effect where the signal drops quickly at offset within ±2 ppm, although residual APT and NOE signals are also present due to partial volume effects. The MTR_{asym} curves from cortex and CC ROIs show the 3.6 ppm APT peaks on top of the distorted negative baseline due to the NOE and MTC_{IM} asymmetry effects (Fig. 2b). In addition to the amide peak, another MT peak can be seen at ~ 2 ppm. Note that in the Z-spectrum, the signal dip at 2 ppm (orange arrow) is much smaller compared to 3.6 ppm due to larger DS effect. At an offset of 5 ppm, the magnitude of MTR_{asym} is much larger than that of

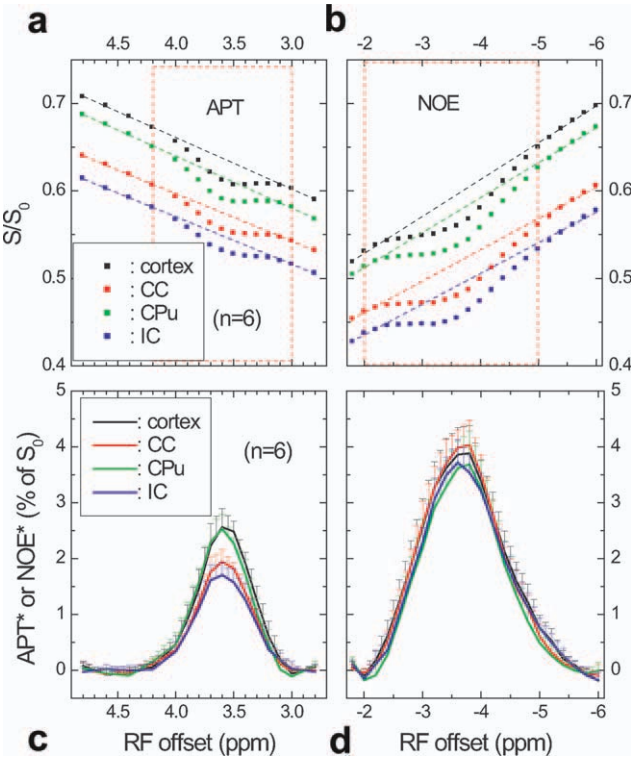

FIG. 3. The APT signals (**a**) from the four selected ROIs span a relatively narrow offset range of 4.2–3.0 ppm, whereas the NOE signals (**b**) appear in a wider offset range of −2.0 to −5.0 ppm. Quantitative APT and NOE can be approximately measured from the difference between a linear fitting of data points outside the red box (dashed lines) and the measured data (squares). Apparent APT (APT*) (**c**) has large contrast in white matter (WM) and gray matter (GM) tissues, whereas apparent NOE (NOE*) (**d**) is similar for all tissue types.

APT and is −10.5 ± 0.5% (n = 6) for CC and −8.1 ± 0.4% for cortex, respectively.

For better visualization of APT and NOE signals, Z-spectra were measured using finer steps in the RF offset (Expt. #1.2). The zoomed Z-spectra obtained from four tissue ROIs (Insets, Fig. 2) show that the APT effect is relatively narrow and mostly falls within the 3.0–4.2 ppm range (Fig. 3a), and the NOE signal spans approximately the −2.0 to −5.0 ppm range (Fig. 3b). Quantitative APT* and NOE* can be approximated from the difference between a linear fit of data points outside the red box (dashed lines) and the data (squares), similar to Fig. 1b. Higher APT* peaks were found at 3.6 ppm for the cortex and CPu ROIs (Fig. 3c) than for the CC and IC ROIs. In contrast, similar NOE* peak magnitudes were found for all four ROIs at about −3.5 to −3.8 ppm (Fig. 3d). Thus, a label offset of 3.6 ppm and −3.5 ppm were chosen for the acquisition of APT* and NOE* maps using Eqs. [3] and [4], respectively.

Estimation of Errors in APT* and NOE*

For both GM and WM with saturation pulse power of 0.6–1.5 μT, the numerically simulated Z-spectra in the offset range of 3.0–4.2 ppm can be well approximated by a linear function (Fig. 4a). In GM, the difference at 3.6 ppm is only 0.1, 0.18, and 0.23% for B_1 values of 0.6, 1.0, and 1.5 μT, respectively. In a wider range of −2.0 to −5.0 ppm used for NOE* calculation (note that symmetric Z-spectra were assumed in the simulation), the line segment between 2.0 and 5.0 ppm deviates from the Z-spectra, and more so for the GM than WM (Fig. 4b). In GM, the difference at 3.5 ppm is 0.8, 1.4, and 1.9% for B_1 values of 0.6, 1.0, and 1.5 μT, respectively. Because DS is related to water R_2, a change in water R_2 mainly affects the Z-spectra within 2 ppm from water resonance, and, therefore, only has a very small effect on the accuracy of APT* (Fig. 4c). Another source of error in APT* or NOE* is the residual APT or NOE effects in the boundary images. In Fig. 4d, the width of the APT effect increases with applied B_1. At the two offsets of 3.0 and 4.2 ppm, the APT signal is minimal for 0.6 μT, but a higher B_1 of 1.5 μT leads to small residual effects, and consequently, more underestimation in APT*.

MTR_{asym}, APT*, and NOE* Maps of Normal Brain (Expts. #1.3–#1.5)

Figure 5 shows maps of MTR_{asym} at 3.6 ppm and 5 ppm, and APT* and NOE* maps (Expts. #1.3 and #1.4).

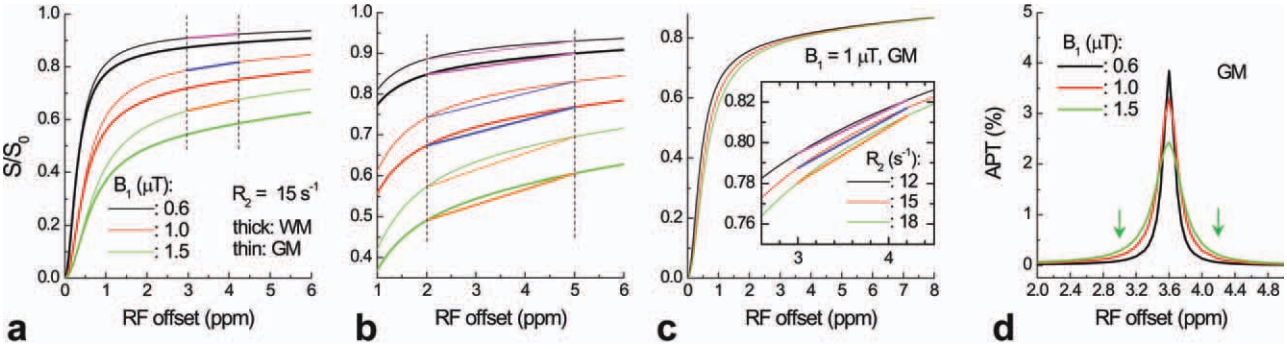

FIG. 4. Z-spectrum signal due to DS and MTC_{IM} effects was simulated for GM and WM at three B_1 levels (**a, b**). In the 3.0–4.2 ppm range (within two dashed lines), the linear approximation holds quite well (line segments vs. Z-spectra curves (a). For a wider range of 2–5 ppm, the linear approximation shows small error for B_1 = 0.6 μT, but the error is larger for two higher B_1 values (b). A change of water R_2 mainly affects the offsets close to the water resonance (**c**). In the 3.0–4.2 ppm range, the difference between Z-spectra curve and line segments increases very slightly with R_2 (inset). A higher saturation power broadens the APT peak (**d**), leading to more residual APT effects in the boundary images.

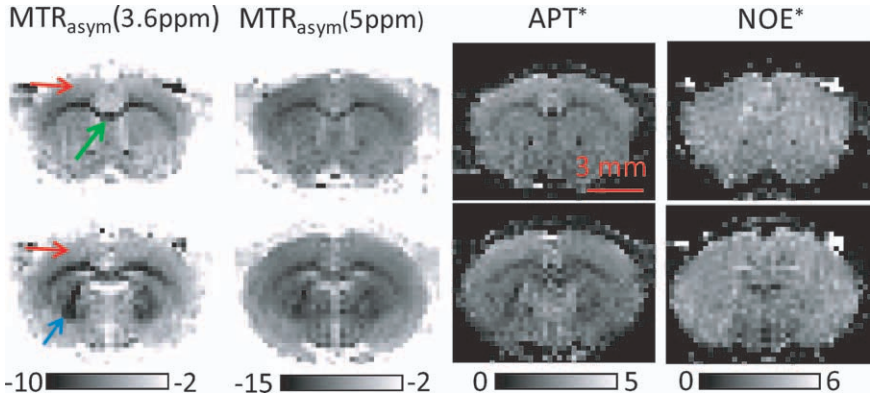

FIG. 5. In vivo maps of MTR_{asym}(3.6 ppm), MTR_{asym}(5 ppm), APT*, and NOE* were obtained from the rat brain for two slices. Note the two MTR_{asym} maps are negative and have similar tissue contrast, where cortex, CC, and IC areas are indicated by red, green, and blue arrows, respectively. The units here are % of S_0.

MTR_{asym}(3.6 ppm) exhibits excellent contrast between cortex (red arrows), CC (green), and IC (blue). Note MTR_{asym} is negative (see Fig. 2b) and its magnitude is significantly higher in WM (CC and IC) than in GM (cortex). Although MTR_{asym}(3.6 ppm) has contributions from APT, NOE, and MTC_{IM} asymmetry, the major contribution of these tissue contrasts actually comes from the MTC_{IM} asymmetry because a quite similar imaging contrast can be seen from the MTR_{asym} map at 5 ppm, which should be mostly out of the APT and NOE range (25,26). The APT* map, although much smaller in magnitude, also shows slight imaging contrasts between GM and WM areas, whereas the NOE* map appears quite homogeneous.

It is known that MTC_{MM} effects, including APT and NOE, are highly dependent on the irradiation pulse parameters (23,36). To find an optimal B_1 and also to examine whether different regional contrasts in APT* and NOE* maps may be due to the specific irradiation pulse we used, B_1-dependency experiments were performed (Expt. #1.5). Figure 6 shows the irradiation power dependence of the APT* and NOE* signals. The optimal B_1 is about 1 μT for APT* and 0.6 μT for NOE*. While the APT* of GM is about 30–40% larger than that of WM for all irradiation powers, the NOE* of GM, interestingly, is slightly smaller (10–20%) than that of WM for $B_1 \leq 1$ μT and the difference diminishes at larger B_1 values.

MTR_{asym}, APT*, and NOE* Maps of Ischemic Brain (Expts. #1.6 and #1.7)

During MCAO, it is known that the APT effect will decrease due to a drop in tissue pH (5,8). Indeed, excellent lesion contrast can be found from the APT* map, which shows very similar lesion size as the ADC map (Fig. 7). Note that within the lesion area, regional heterogeneity (red vs. yellow arrow) can be seen from the quantitative APT* map, which may indicate different pH values. Although the lesion area can also be observed from the MTR_{asym}(3.6 ppm) map, the contrast of the ipsilateral side versus the contralateral side is similar to (red vs. blue) or smaller than (green vs. blue) the contrast between normal GM and WM tissues. The weaker sensitivity of MTR_{asym}(3.6 ppm) compared to the APT* map is partly due to there being almost no lesion contrast in the maps of NOE* and MTC_{IM} (represented by MTR_{asym} (5 ppm)), the major contributors to the MTR_{asym} map.

The contrast of APT* and MTR_{asym}(3.6 ppm) between ischemic and normal brain regions was quantified. Figure 8b shows averaged APT* and MTR_{asym}(3.6 ppm) for WM ROI (purple in 8a), and the contralateral normal (red contour in 8a) and ipsilateral ischemic (green contour in 8a) CPu ROIs. Although the magnitude of APT* is generally much smaller than MTR_{asym}, the magnitude of lesion contrast in APT* (between contralateral and ipsilateral CPu) is 1.86 ± 0.27%, similar to that of MTR_{asym}, 2.00 ± 0.32% (paired t-test, $P > 0.1$). The lesion contrast in APT* is much larger than the contrast of APT* in contralateral CPu versus WM ($P < 5 \times 10^{-6}$), whereas the lesion contrast in MTR_{asym} is similar to the contrast between contralateral CPu and WM ($P > 0.1$). In the APT* maps (Fig. 7), heterogeneous intensities were observed within the ischemic region. To determine the relationship between APT* and ADC, a scatter plot was obtained for all pixels in a large lesion ROI (yellow contour, Fig. 8a) from all MCAO rats (Fig. 8c). Clearly, highly positive correlation was observed ($R = 0.70 \pm 0.10$, $n = 7$ animals). However, NOE* is nearly

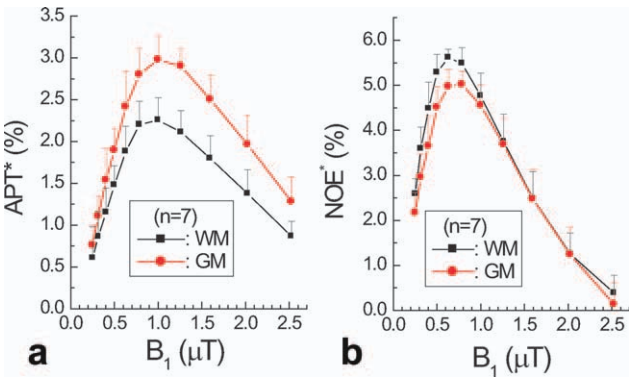

FIG. 6. Averaged APT* (**a**) and NOE* (**b**) values as a function of B_1. APT* of GM is about 30–40% higher than WM. NOE* is about 10–20% higher for WM than GM at lower irradiation pulse power, but the contrast between WM and GM diminishes at larger B_1.

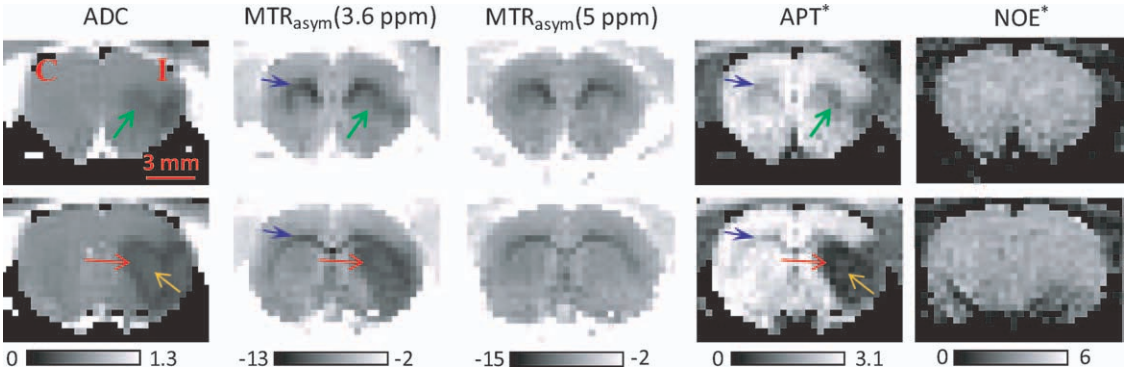

FIG. 7. ADC, MTR_{asym} at 3.6 ppm, 5 ppm, APT*, and NOE* maps from a representative rat following MCAO. MTR_{asym}(5 ppm) and NOE* have almost no contrast between ipsilateral versus contralateral sides. C: contralateral, I: ipsilateral. MTR_{asym}(3.6 ppm) map can detect large and severe lesions but has difficulty detecting smaller ones (red vs. green arrows). The quantitative APT* map can detect lesion areas similar to the ADC map, and the APT and ADC maps are correlated well in space (red and green arrows). Moreover, APT* can also distinguish regional heterogeneity within the lesion area (red vs. yellow arrows), similar to ADC.

independent of ADC ($R = 0.16 \pm 0.25$), indicating that NOE* is not sensitive to pH, unlike APT.

Contribution of Chemical Exchange to the NOE Signal (Expts. #2.1 and 2.2)

Theoretically, MTC_{MM} is proportional to the concentration of mobile macromolecule as well as the MT rate (5,23). Although no ischemic contrast was found for NOE*, suggesting its pH-independence, one cannot exclude the possibility that there were concomitant significant changes in MT rate and the mobile macromolecule content (37), and that the two effects cancel each other. To examine the pH effect and concentration dependence of NOE separately, BSA phantoms were measured and the results are shown in Fig. 9. For both $B_1 = 0.5$ and 1.0 μT, the CEST signals exhibited clear pH-dependence: sharp dips occurred at about 2.8 ppm for pH ≤ 6.4, and the dip was smaller and broader for pH = 7.0 (Fig. 9a). The upfield NOE signals, in contrast, were almost identical for all samples indicating that the NOE of BSA is insensitive to the chemical exchange in the pH = 5.0–7.0 range. As expected, both NOE and CEST signals in the Z-spectra were proportional to the BSA concentration (Fig. 9b). The dependence on the concentration could also be appreciated from the NOE* map obtained using three offset measurements of −2.0, −3.5, and −5.0 ppm (inset). Figure 9c shows the Z-spectra of the 20% BSA (pH = 7.0) sample with six B_1 values, where the optimal B_1 maximizes the NOE signal at around 0.5 μT (Fig. 9c), similar to the optimal B_1 of 0.6 μT in rat studies observed in Fig. 6. The NOE signal nearly diminishes with a 2 μT saturation pulse, which is similar to the B_1 dependence of NOE in BSA phantoms reported by Hubbard et al. (38).

DISCUSSIONS

Our results can be summarized as (i) that Z-spectra obtained at a high field of 9.4 T have two narrow CEST peaks at ∼ 3.6 and ∼ 2.0 ppm and a broader NOE peak in the −2.0 to −5.0 ppm range, (ii) the MTC_{IM} asymmetry and NOE are significant contributors to the MTR_{asym} analysis of APT, (iii) HR APT* and NOE* maps can be obtained at a high field by simple three-offset measurements, (iv) APT* is sensitive to ischemia, whereas NOE*

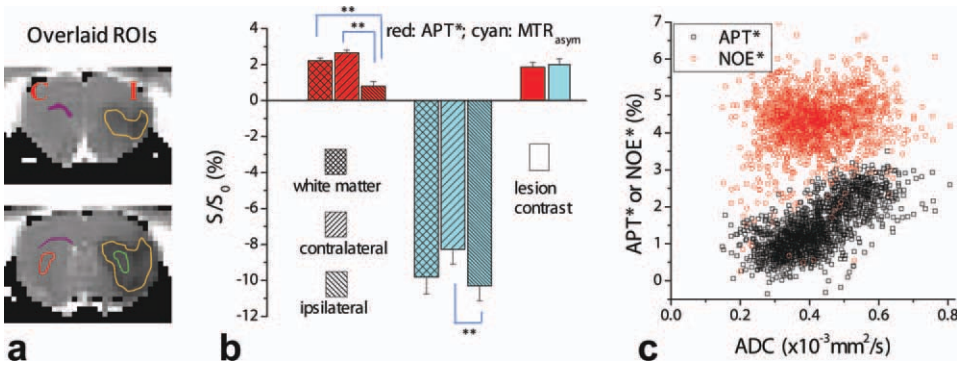

FIG. 8. **a**: The contours overlaid on the ADC maps of a representative rat indicate ROIs used for quantitative data analysis. **b**: Comparison of the averaged ($n = 7$) APT* and MTR_{asym} (3.6 ppm) from the WM (purple in a), the contralateral (red in a) and ipsilateral (green in a) CPu ROIs. The lesion contrast is calculated from the difference between contralateral and ipsilateral CPu data. The symbol ** indicates $P < 1 \times 10^{-5}$ from a paired Student's *t*-test. b: The scatter plot of APT* and NOE* versus ADC values obtained from pixels in a large lesion ROI (yellow in a) from all animals. APT* values are highly correlated with ADC whereas NOE* values are almost independent of ADC.

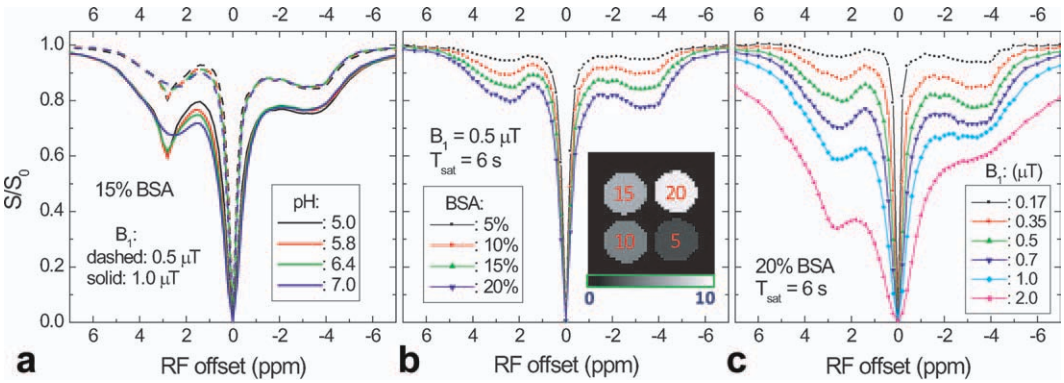

FIG. 9. Z-spectra of (**a**) 15% BSA phantoms with different pH values measured with 0.5 and 1.0 μT saturation pulses, (**b**) BSA phantoms with different concentrations measured with a 0.5 μT saturation pulse, and (**c**) 20% BSA phantom measured with six different B_1 pulses. The NOE* map from the three offset measurement for $B_1 = 0.65$ μT is shown in the inset, where the concentration in percentage is labeled in red and the unit of the gray scalebar is % of S_0.

and MTC_{IM} are not, and (v) NOE of BSA phantoms is proportional to the macromolecule concentration but is insensitive to chemical exchange.

Z-Spectrum and MTR_{asym} Analysis

To investigate the MT process between water and mobile macromolecules, van Zijl et al. had performed water-exchange-filter experiments (WEX) where water magnetization was selectively labeled and transferred to other molecules (26), in a reversed way to the saturation transfer experiments. In their in vivo and postmortem water-exchange-filter experiment spectra from rat brain, a small peak at $\sim$ 2 ppm downfield from water and several upfield aliphatic peaks were observed besides the APT peak, similar to the peaks observed in our Z-spectra. The width of the APT peak is about 1 ppm, which is similar to our results of 1.2 ppm. The origin of the $\sim$ 2 ppm peak is still uncertain and has been attributed to mobile lipids (26) or amide of glutamine and glutamine residues in protein (25). Whereas water-exchange-filter experiment measures the mobile macromolecules directly and has better spectral resolutions, a saturation transfer experiment measures the water signal and has much enhanced sensitivity, which is crucial for imaging the small APT and NOE signals.

The MTR_{asym} maps have usually been acquired for APT-weighted imaging. However, the APT contribution to MTR_{asym} is small compared to the MTC_{IM} asymmetry and upfield NOE signal. Unlike our APT* map, in the MTR_{asym} map, the contrast between ischemic versus normal tissue is often similar to or smaller than the regional variance of normal tissues (see blue vs. red and green arrows in Fig. 7), reducing the sensitivity of detecting pathological changes. The problem of quantifying APT by MTR_{asym} has been realized by many researchers, and several approaches have been proposed to address this issue. Scheidegger et al. applied two selected saturation pulse powers at both the amide frequency of 3.5 ppm and the reference frequency of −3.5 ppm to extract the APT effect, assuming that APT would be equal for both powers whereas the DS and MTC_{IM} effects linearly increase with the saturation power (39). An advantage of this approach is that it is insensitive to the B_0 inhomogeneity (39), but it may not be able to separate the APT from NOE because the MT rate of NOE is slower than APT (26) and, thus, NOE can be saturated at a smaller power level than APT. Recently, Jones et al. proposed to use pulsed saturation in a three-dimensional imaging sequence and the CEST data is obtained at the steady state (20). To extract the APT, a very low power irradiation pulse (equivalent to a 0.4 μT continuous wave pulse) was chosen to minimize the MTC_{IM}, and the DS effect is fitted from the Z-spectra with a Lorentzian function. However, sampling a wide Z-spectrum reduces the scanning efficiency because the APT signal is only contained in the narrow range around 3.6 ppm (26).

Three Offset Measurement Approach for APT and NOE

At a high magnetic field of 9.4 T, we showed that APT* and NOE* maps can be acquired simply with measurements at three offsets, which can be considered as an extreme simplification of the Z-spectrum fitting for the APT and NOE. Our in vivo APT* data should have only a small quantification error because (i) the magnitude of APT matches well with literature values reported by other groups (5,14), (ii) a linear function is a good approximation of Z-psectra within 3.0–4.2 ppm, based on simulation results of APT, and (iii) the magnitude of ischemic APT* contrast is nearly equal to that of MTR_{asym} (Fig. 8b). Similar to our APT* approach of three offsets (3.0, 3.6, and 4.2 ppm), Sun et al. recently proposed to use three offsets of 2.0, 3.5, and 5.0 ppm for obtaining APT-weighted maps (11). The width of APT resonance is only 1–1.2 ppm from our results as well as the water-exchange-filter experiment spectrum (26), thus two reference scans of 2.0 and 5.0 ppm would increase the quantification error. Moreover, the 2.0 ppm scan has significant MT contribution from nonamide protons [Fig. 2 and also Ref. 26], which may contaminate the results. Compared to APT*, which should be a good surrogate of APT, the NOE* results have a larger quantification error due to its wider offset range. At an irradiation power of 0.6 μT, the linear assumption underlying the three offset method underestimates the NOE signal by 0.8%, or about

15% of the NOE* signal. In addition, the aliphatic region observed by NMR spectroscopy is wider and also closer to the water (24–26). Therefore, the −2.0 ppm chosen as a boundary offset here likely contains residual NOE effects, leading to a greater underestimation in our NOE* results. Further systematic evaluations are needed to determine the accuracy of using NOE* as a surrogate of NOE.

The three offset measurement relies on clear delineation of the APT and NOE peaks, therefore, a high magnetic field is beneficial, and the bandwidth of the saturation pulse should be kept as narrow as possible. In our study a 3–4 s continuous wave pulse was used. For clinical scanners, however, a long irradiation pulse is often unavailable and short saturation pulse trains have been used instead. For very short saturation pulses, the peaks and boundaries of APT and NOE may not be well defined, leading to quantification errors. In addition, a good shimming and B_0 field homogeneity is critical for accurate determination of the APT and NOE peaks. Although the three offset measurement may be difficult to achieve at field strengths of 3 T or lower, our results should still be applicable to 7 T, where the offsets and the optimal saturation pulse may need slight adjustments, and would result in only a slightly increased quantification error. Further studies using simulations or phantom experiments will be helpful to evaluate the validity of the three offset measurement at lower fields and the minimum pulse length necessary for pulse trains to obtain three offset APT* and NOE* mapping with acceptable accuracy.

Sources of APT and NOE Signals

Although APT and NOE both reflect MT effect from mobile macromolecules, GM has larger APT* and smaller NOE* than WM, indicating somewhat different signal origins (Fig. 6). Taking into account that the MTC_{MM} is proportional to water T_1, which is $\sim$ 20% longer in GM than WM at 9.4 T (40), and assuming that the MT exchange rate of APT and NOE are similar in gray and white matters, the population of mobile macromolecule protons will be about 10–20% higher in GM for APT* and 30–40% higher in WM for NOE*, respectively. Therefore, one may postulate that APT mainly arises from mobile proteins and peptides that have a slightly higher concentration in GM, whereas NOE, in addition to mobile proteins and peptides, has contributions from mobile lipid, which may have a much higher concentration in WM.

Our MCAO and phantom experiments indicate that pH has minimal effect on NOE, unlike APT. Similar conclusions can be made from previous Z-spectra showing a minimal difference in the upfield NOE frequencies between ischemic brain and normal control (5,11,13). Little ischemic contrast in NOE is also in agreement with the notion that there is little change in the concentration of mobile proteins during initial hours of ischemia, whereas the large drop in APT magnitude is mostly due to the decrease of exchange rate (5). Thus, NOE can provide a valuable imaging index of mobile macromolecular concentration and is complementary to APT.

CONCLUSIONS

To circumvent the problem of APT quantification using the asymmetry analysis, the wide spectral separation associated with a high magnetic field can be exploited for direct mapping of the APT as well as the NOE signal. HR maps obtained from the three offset measurement show that the apparent APT is larger in GM than WM and is highly sensitive to tissue acidosis. The magnitude of NOE* is much higher than APT*, but it has less regional heterogeneity across brain and is insensitive to pH. With direct imaging of APT* and NOE*, these contrasts can potentially provide complementary quantitative information regarding pH and mobile macromolecule concentrations and gives more insight and opens new opportunities in pathological applications.

ACKNOWLEDGMENTS

The authors thank Kristy Hendrich for magnet management and Dr. Alex Poplawsky for proofreading.

REFERENCES

1. Wolff SD, Balaban RS. Magnetization transfer contrast (MTC) and tissue water proton relaxation in vivo. Magn Reson Med 1990;10:135–144.
2. Pike GB, Hu BS, Glover GH, Enzmann DR. Magnetization transfer time-of-flight magnetic resonance angiography. Magn Reson Med 1992;25:372–379.
3. Dousset V, Grossman RI, Ramer KN, Schnall MD, Young LH, Gonzalez-Scarano F, Lavi E, Cohen JA. Experimental allergic encephalomyelitis and multiple sclerosis: lesion characterization with magnetization transfer imaging. Radiology 1992;182:483–491.
4. Ward KM, Aletras AH, Balaban RS. A new class of contrast agents for MRI based on proton chemical exchange dependent saturation transfer (CEST). J Magn Reson 2000;143:79–87.
5. Zhou JY, Payen JF, Wilson DA, Traystman RJ, van Zijl PCM. Using the amide proton signals of intracellular proteins and peptides to detect pH effects in MRI. Nat Med 2003;9:1085–1090.
6. Zhou JY, Tryggestad E, Wen ZB, Lal B, Zhou TT, Grossman R, Wang SL, Yan K, Fu DX, Ford E, Tyler B, Blakeley J, Laterra J, van Zijl PCM. Differentiation between glioma and radiation necrosis using molecular magnetic resonance imaging of endogenous proteins and peptides. Nat Med 2011;17:130–U308.
7. Jia GA, Abaza R, Williams JD, Zynger DL, Zhou JY, Shah ZK, Patel M, Sammet S, Wei L, Bahnson RR, Knopp MV. Amide proton transfer mr imaging of prostate cancer: a preliminary study. J Magn Reson Imaging 2011;33:647–654.
8. Sun PZ, Zhou JY, Sun WY, Huang J, van Zijl PCM. Detection of the ischemic penumbra using pH-weighted MRI. J Cereb Blood Flow Metab 2007;27:1129–1136.
9. Jokivarsi KT, Grohn HI, Grohn OH, Kauppinen RA. Proton transfer ratio, lactate, and intracellular pH in acute cerebral ischemia. Magn Reson Med 2007;57:647–653.
10. Zhou JY, Blakeley JO, Hua J, Kim M, Laterra J, Pomper MG, van Zijl PCM. Practical data acquisition method for human brain tumor amide proton transfer (APT) imaging. Magn Reson Med 2008;60:842–849.
11. Sun PZ, Benner T, Copen WA, Sorensen AG. Early experience of translating ph-weighted mri to image human subjects at 3 Tesla. Stroke 2011;41:S147–S151.
12. Hua J, Jones CK, Blakeley J, Smith SA, van Zijl PCM, Zhou JY. Quantitative description of the asymmetry in magnetization transfer effects around the water resonance in the human brain. Magn Reson Med 2007;58:786–793.
13. Jin T, Wang P, Zong X, Kim SG. Magnetic resonance imaging of the amine-proton EXchange (APEX) dependent contrast. Neuroimage 2012;59:1218–1227.
14. Sun PZ, Zhou JY, Huang J, van Zijl P. Simplified quantitative description of amide proton transfer (APT) imaging during acute ischemia. Magn Reson Med 2007;57:405–410.
15. Kumar A, Ernst RR, Wuthrich K. A two-dimensional nuclear overhauser enhancement (2d Noe) experiment for the elucidation of complete proton-proton cross-relaxation networks in biological macromolecules. Biochem Biophys Res Commun 1980;95:1–6.

16. Kumar A, Wagner G, Ernst RR, Wuthrich K. Buildup rates of the nuclear overhauser effect measured by two-dimensional proton magnetic-resonance spectroscopy—implications for studies of protein conformation. J Am Chem Soc 1981;103:3654–3658.
17. Bothnerby AA, Stephens RL, Lee JM, Warren CD, Jeanloz RW. Structure determination of a tetrasaccharide—transient nuclear overhauser effects in the rotating frame. J Am Chem Soc 1984;106:811–813.
18. Ling W, Regatte RR, Navon G, Jerschow A. Assessment of glycosaminoglycan concentration in vivo by chemical exchange-dependent saturation transfer (gagCEST). Proc Natl Acad Sci USA 2008;105: 2266–2270.
19. Mougin OE, Coxon RC, Pitiot A, Gowland PA. Magnetization transfer phenomenon in the human brain at 7 T. Neuroimage 2010;49:272–281.
20. Jones CK, Polders D, Huang W, Zhu H, Hoogduin HJ, Zhou JY, Luijten P, Van Zijl P. In vivo three-dimensional whole-brain pulsed steady-state chemical exchange saturation transfer at 7 T. Magn Reson Med 2011. doi: 10.1002/mrm.23141.
21. Kauppinen RA, Kokko H, Williams SR. Detection of mobile proteins by proton nuclear magnetic resonance spectroscopy in the guinea pig brain ex vivo and their partial purification. J Neurochem 1992;58:967–974.
22. Behar KL, Ogino T. Characterization of macromolecule resonances in the 1H NMR Spectrum of rat brain. Magn Reson Med 1993;30:38–44.
23. van Zijl PCM, Yadav NN. Chemical exchange saturation transfer (CEST): what is in a name and what isn't? Magn Reson Med 2011;65: 927–948.
24. Akasaka K, Konrad M, Goody RS. Selective spin diffusion—novel method for studying motional properties of biopolymers in solution. FEBS Lett 1978;96:287–290.
25. Mori S, Eleff SM, Pilatus U, Mori N, van Zijl PCM. Proton NMR spectroscopy of solvent-saturable resonances: a new approach to study pH effects in situ. Magn Reson Med 1998;40:36–42.
26. van Zijl PCM, Zhou JY, Mori N, Payen JF, Wilson D, Mori S. Mechanism of magnetization transfer during on-resonance water saturation. A new approach to detect mobile proteins, peptides, and lipids. Magn Reson Med 2003;49:440–449.
27. Henkelman RM, Stanisz GJ, Graham SJ. Magnetization transfer in MRI: a review. NMR Biomed 2001;14:57–64.
28. Jones CK, Huang AJ, van Zijl PCM. Exchange-relayed nuclear Overhausser effect MRI. In: Proc 19th ISMRM Annual Meeting. Montreal, Canada; 2011. p 2735.
29. Vandeven FJM, Janssen H, Graslund A, Hilbers CW. Chemically relayed nuclear overhauser effects - connectivities between resonances of nonexchangeable protons and water. J Magn Reson 1988;79: 221–235.
30. Morrison C, Stanisz GJ, Henkelman RM. Modeling magnetization transfer for biological-like systems using a semi-solid pool with super-Lorentzian lineshape and dipolar reservoir. J Magn Reson B 1995;108:103–113.
31. Morrison C, Henkelman RM. A model for magnetization transfer in tissue. Magn Reson Med 1995;33:475–482.
32. Li AX, Hudson RHE, Barrett JW, Jones CK, Pasternak SH, Bartha R. Four-pool modeling of proton exchange processes in biological systems in the presence of MRI-paramagnetic chemical exchange saturation transfer (PARACEST) agents. Magn Reson Med 2008;60:1197–1206.
33. Jin T, Kim S-G. Change of the cerebrospinal fluid volume during brain activation investigated by T1ρ-weighted fMRI. Neuroimage 2010;51:1378–1383.
34. Kiozumi J, Yoshida Y, Nakazawa T, Ooneda G. Experimental studies of ischemic brain edema: I: a new experimental model of cerebral embolism in rats in which recirculation can be introduced in the ischemic area. Jpn J Stroke 1986;8:1–8.
35. Kim M, Gillen J, Landman BA, Zhou JY, van Zijl PCM. Water saturation shift referencing (WASSR) for chemical exchange saturation transfer (CEST) experiments. Magn Reson Med 2009;61: 1441–1450.
36. Sun PZ, van Zijl PCM, Zhou JY. Optimization of the irradiation power in chemical exchange dependent saturation transfer experiments. J Magn Reson 2005;175:193–200.
37. Hakumaki JM, Grohn OH, Pirttila T-RM, Kauppinen RA. Increased macromolecular resonances in the rat cerebral cortex during severe energy failure as detected by 1H nuclear magnetic resonance spectroscopy. Neurosci Lett 1996;212:151–154.
38. Hubbard PL, Narvainen J, Kauppinen RA, Morris GA. Unexpected Magnetization Transfer to Aliphatic Resonances in Z-Spectroscopy in Model Systems and In Vivo. In: Proceedings of the 15th ISMRM Annual Meeting, Berlin, Germany; 2007. p 3464.
39. Scheidegger R, Vinogradov E, Alsop D. Amide proton transfer imaging with improved robustness to magnetic field inhomogeneity and magnetization transfer asymmetry using saturation with frequency alternating RF irradiation. Magn Reson Med 2011;66:1275–1285.
40. Kuo YT, Herlihy AH, So PW, Bhakoo KK, Bell JD. In vivo measurements of T_1 relaxation times in mouse brain associated with different modes of systemic administration of manganese chloride. J Magn Reson Imaging 2005;21:334–339.